Journal of Engineering Science and Technology Review 18 (2) (2025) 58- 66

Research Article

JOURNAL OF
Engineering Science and Technology Review

www.jestr.org

Study of Friction Stir Welding of Aluminum Alloy 6063 Pipes and the Weld Microstructure and Mechanical Properties

Worapong Boonchouytan*

Department of Industrial Engineering, Faculty of Engineering, Rajamangala University of Technology Srivijaya, Songkhla, 90000, Thailand

Received 29 October 2024; Accepted 22 March 2025

Abstract

The objectives of this study were to examine the mechanical resistance of welds and to characterize their macro- and microstructures for potential industrial applications. In this study, friction stir welding experiments were conducted using an aluminum alloy AA6063 pipe with an outer diameter of 50.8 mm and an inner diameter of 38.85 mm. The friction stir welder used in this study had a triangular cylindrical shape. The pin measured 6 mm in diameter, 4.8 mm in height, and had a shoulder diameter of 20 mm. This welder was equipped with an inverter and a motor for automatic adjustment of the dividing plate's rotation speed. Experiments were conducted at three rotation speeds (710, 1000, and 1400 rpm) and three travel speeds (1.5, 2.5, and 3.5 mm/min). Macro- and microstructural characterization, as well as hardness and tensile tests, were then performed. According to the results, small cracks were observed in the welds in the stir zone (SZ) region, primarily due to excessive frictional heat accumulation between the material and the welder. This accumulation caused stress, resulting in tunnel formation within the material. Excessive rotation speed and high travel speed of the welder led to abnormal material stirring and a steep temperature gradient in the thickness direction. This abnormal stirring created flow separation, leading to a gap on the advancing side (AS). At low rotation speeds and high travel speeds, tunnel defects were mainly formed due to insufficient heat input. Friction stir welding at a rotation speed of 1000 rpm and a travel speed of 1.5 mm/min demonstrated the highest tensile strength at 152.17 MPa. The highest hardness, recorded at 57.3 HV, was achieved at a rotation speed of 1400 rpm and a travel speed of 2.5 mm/min.

Keywords: Friction stir welding, Aluminum alloy 6063, Pipes, Mechanical properties

1. Introduction

Aluminum 6063 is classified as an aluminum alloy, primarily composed of magnesium and silicon. It can be machined through heat treatment when these components meet the required specifications. While its durability may not match that of aluminum grades in the 2000 or 7000 series, Aluminum 6063 is relatively easy to machine into various shapes and is considered a common grade of aluminum. Due to its machinability, it is widely used in applications such as automotive parts, joints, spare components, turning, welding, and piping.

Significant opportunities exist to meet the growing demands of industries such as aerospace, automotive, and supercritical power plants, driven by advancements in materials research and friction stir welding (FSW). FSW is a solid-state welding process that avoids the drawbacks of traditional fusion welding, which can introduce issues related to heat and high temperatures. The material processing, alloy composition, and pre-welding heat treatment of aluminum alloy grades influence variations in microstructure, grain size, and defects, ultimately affecting the material's properties [1]. The development of thicker welds in pipe welding remains essential in welding technology research, even with advancements in solid-state material joining. Furthermore, a recent study by The Welding Institute (TWI) suggests that friction stir welding may offer a more economical solution for joining thicker sections [2]. Although FSW is relatively slower than conventional arc welding, it can weld thicker sections of large structures such as oil and gas pipelines, offshore platforms, and heavy machinery in a single pass, resulting in significant cost savings.

Pipes are often welded using fusion welding techniques. A primary issue with fusion welding is the increased heat input, which softens the base metal and reduces its tensile strength [3]. The heat input in FSW is lower than that in fusion welding processes because it is a solid-state welding method. This reduces the malleability of the base metal and enhances the strength of the weld [3]. FSW for pipe welding presents several challenges, including frictional heating at the interface where the underside of the welder contacts the curved surface of the pipe, as well as the placement of the pipe clamping device. Numerous studies have explored the use of FSW for welding pipelines. For example, research on the FSW of AA6061 pipes with an outer diameter of 107 mm and a thickness of 5.1 mm found no defects in the weld macrostructure and achieved a maximum welding efficiency of 70% at a rotation speed of 1600 rpm and a travel speed of 355 mm/min [4]. Tensile strength testing indicated that none of the specimens exhibited fractures in the weld zone after the friction stir welding of copper and aluminum pipes with thicknesses of 1.5 mm and 1 mm, respectively [5]. Compared to single-pass welding, the friction stir welding of AA6082 pipes with an outer diameter of 38 mm, utilizing a two-pass welding technique along with the removal of holes at the end of the weld using a telescopic pin, resulted in a defect-free weld [6]. Using triangular frustum pins, friction stir welding of pipes resulted in defect-free welds at a travel speed of 40

*E-mail address: worapong.b@rmutsv.ac.th
ISSN: 1791-2377
doi:10.25103/jestr.182.08

mm/min and rotation speeds of 600 and 800 rpm. However, there are still no reports on the welding of AA6063 pipes, despite extensive research on friction stir welding.

This study aimed to enhance the understanding of the mechanical resistance of welds and their macro- and microstructural characteristics for future industrial applications. It examined the friction stir welding of AA6063 pipes with a diameter of 50.8 mm and a wall thickness of 12 mm at varying rotation and travel speeds, using hardness and tensile strength tests.

2. Methodology

2.1 Materials and Welder

The materials used in the friction stir welding experiments were aluminum alloy AA6063 pipes with an outer diameter of 50.8 mm and an inner diameter of 38.85 mm. The chemical composition and mechanical properties of the pipes are presented in Table 1.

Table 1. Chemical composition and mechanical properties of the materials used in the experiments.

Si	Fe	Cu	Mn	Mg	Cr	Zn	Ti	Al
0.50	**0.35**	**0.10**	**0.10**	**0.90**	**0.10**	**0.10**	**0.10**	**Balance**
Tensile Strength (MPa)			Elongation (%)			Hardness Vickers (HV)		
225			11			52		

The welder featured a cylindrical shape with triangular threads, as shown in Fig. 1. The pin had a diameter of 6 mm, a height of 4.8 mm, and a shoulder diameter of 20 mm. It was made of H13 hot-forged mold steel, exhibiting a hardness of 59 HRC after annealing. The welder was mounted in the spindle of the OBRAECI STROJE vertical milling machine, model FGV 32.

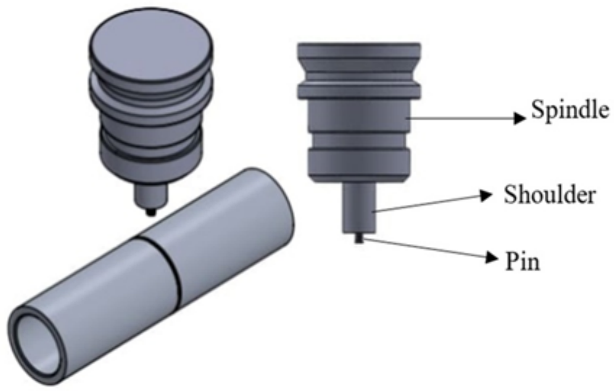

Fig. 1. Stirring tool.

2.2 Friction Stir Welder for Pipes

The friction stir welder was equipped with an inverter and a motor for automatic adjustment of the rotation speed of the dividing plate (1). The dividing plate was mounted on the vertical milling machine and driven by a transmission motor (2). A support system was in place to provide compression during the welding of the specimen (3). The aluminum specimen at the lathe center was secured by the tailstock (4), as shown in Fig. 2.

The two experimental factors included three rotation speeds (710, 1,000, and 1,400 rpm) and three travel speeds (1.5, 2.5, and 3.5 mm/min). Welding was initiated by pressing the start button on the control panel of the vertical milling machine to rotate the pin, followed by pressing the start button to send power from the motor to automatically rotate the dividing plate at the specified speed.

2.3 Friction Stir Welding of Pipes

The friction stir welding of pipes under all experimental conditions in this study consisted of the following steps:

(a) Turn on the vertical milling machine to rotate the pin clockwise.

(b) Insert the pin into the material until the tip of the pin reaches the specified depth and hold it there for 30 seconds, allowing the aluminum to soften and circulate around the pin before proceeding with welding at the specified speed.

(c) The heat generated from the friction between the pin's surface and the shoulder softens the material and creates a swirling motion around the pin.

(d) Continue welding at the specified travel speed, during which material aggregation occurs.

(e) A joint is formed.

(f) At the end of the welding process, before lifting the pin out of the weld, maintain a constant friction at the final position for about 30 seconds, as shown in Fig. 3.

Fig. 2. Friction stir welder for cylindrical specimens.

2.4 Characterization of Metallurgical Structure and Mechanical Properties of the Welds

Macro and Micro Structural Examination: After the welding was completed, an initial visual inspection of the welds revealed no defects. To conduct a detailed examination, the specimens were cast in epoxy resin and then cut into a standard shape, as shown in Fig. 4. The specimens were polished using wet sandpapers ranging from No. 320 to No. 1500 to achieve the required level of smoothness. Following this, they were further polished with alumina powder of particle sizes 3 µm, 0.5 µm, and 0.1 µm, respectively.

Hardness Test: The specimens for the hardness test were shaped identically to those used in the macro- and micro-structural examinations. The Vickers hardness test was conducted by applying a compression force to the cross-section of the weld, with a span length of 1 mm and a compression force of 100 gf for a duration of 10 seconds.

Tensile Test: The tensile test is used to determine the strength of materials under tensile loads or forces, utilizing specimens prepared according to the ASTM-B557M standard test methods, as shown in Fig. 5. In this study, the specimens obtained from friction stir welding were cut crosswise to the weld line to evaluate the weld strength at room temperature, with a tensile speed of 1 mm/min.

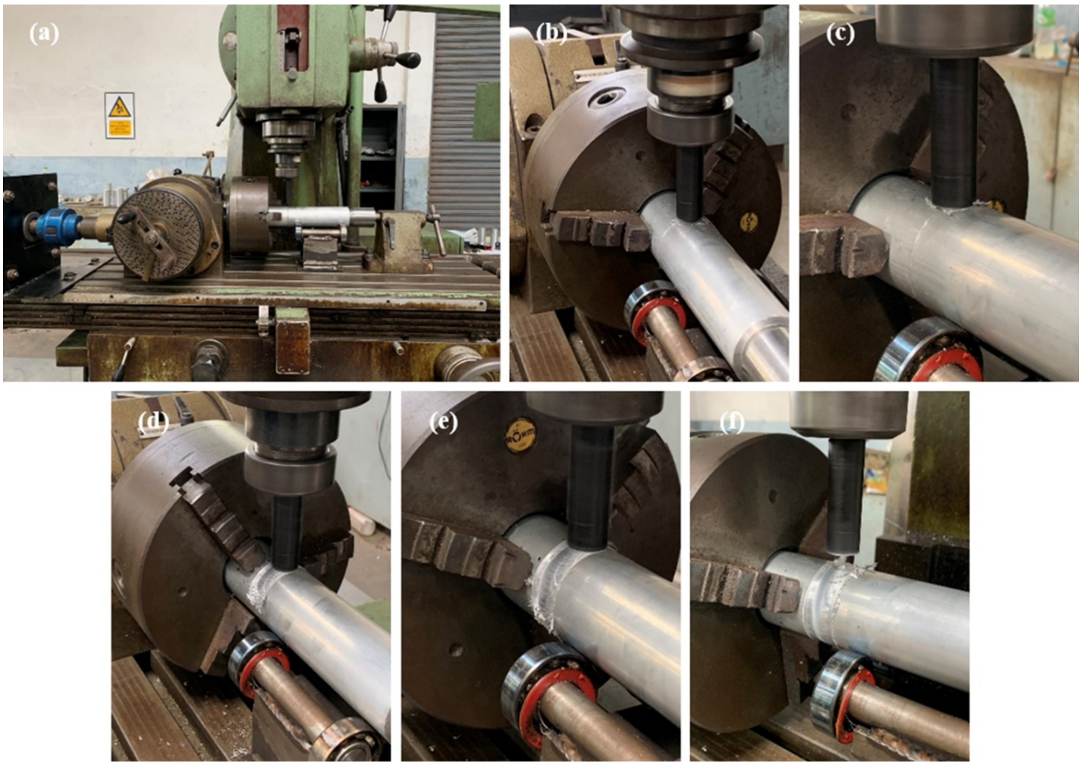

Fig. 3. Friction stir welding process. (a) Turn on the vertical milling machine; (b) Insert the pin into the material; (c) Rotate the pin against the material; (d) Weld at the specified travel speed; (e) Stop the pin upon cycle completion; and (f) Lift the pin out of the material.

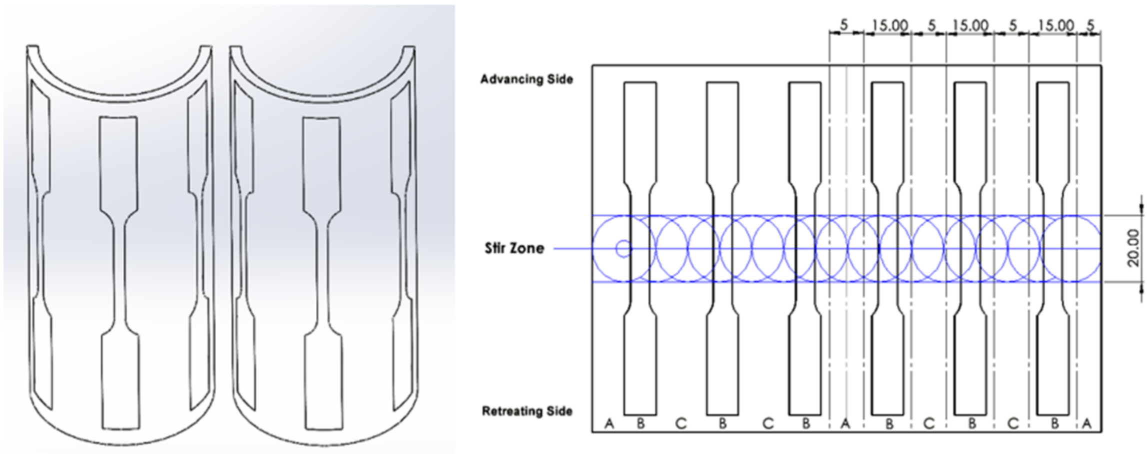

Fig. 4. Location of points for characterization of metallurgical and mechanical properties of the welds.

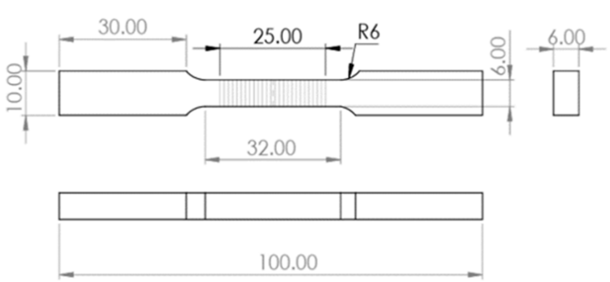

Fig. 5. Specimen prepared according to ASTM-B557M standard test methods.

3. Results and Discussion

3.1 Top Surface of the Welds

According to the characterization of the top surface of the welds obtained from the friction stir welding process, as shown in Fig. 6, the weld surfaces demonstrated good integration at the butt joints, and the bottom of the welds exhibited deep penetration without any non-integrated cracks. However, holes were observed at the end of the welds due to the tip of the pin (Fig. 6(a)). The welds produced at rotation speeds of 1400 rpm (Fig. 6(d)), 1000 rpm (Fig. 6(c)), and 710 rpm (Fig. 6(b)) displayed a smoother surface. This smoother surface is attributed to the fact that the surface layer of the welded specimen formed in alignment with the laminar material flow, while internal friction caused intermittent material flow, resulting in a more pronounced shoulder on the weld surface [7].

3.2 Macro and Microstructure of the Welds

Fig. 7-9 display the microstructure of the welds at rotation speeds of 710, 1000, and 1400 rpm, respectively. Only the welds produced at a travel speed of 1.5 mm/min are presented, as other travel speeds yielded comparable results. Clear zones, including the Stir Zone (SZ), the Thermo-Mechanically Affected Zone (TMAZ), the Heat Affected Zone (HAZ), and the Base Metal (BM), were visible in the macrostructure of the welds across all three rotation speeds [8]. These zones became more pronounced at higher cooling rates of the welds and lower plastic flow of the metal [9]. Furthermore, due to dynamic recrystallization that occurred during the friction stir welding process, the SZ region exhibited a fine and balanced grain structure. In contrast, the grains in the TMAZ Advancing Side (AS) and TMAZ Retreating Side (RS) regions displayed a highly distorted structure of the aluminum matrix, with significant elongation in the grains resulting from the stress generated in these areas during the friction stir welding process [10].

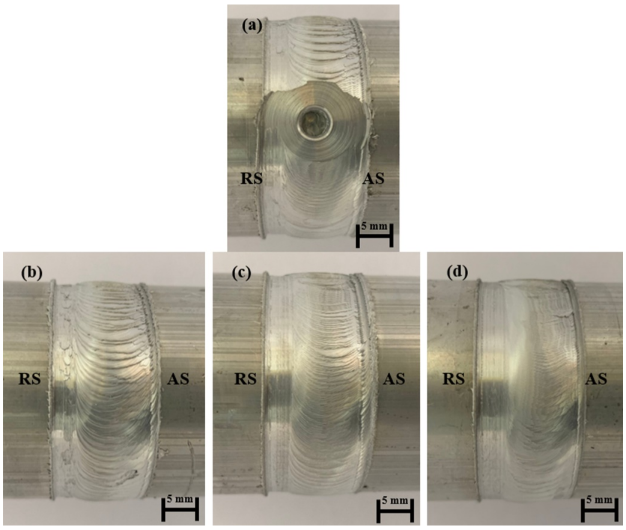

Fig. 6. Surface topography of friction stir welds.(a) Start and end of welding; (b) Rotation speed of 710 rpm; (c) Rotation speed of 1000 rpm; and (d) Rotation speed of 1400 rpm.

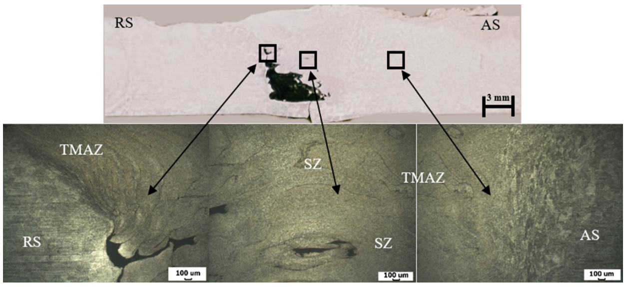

Fig. 7. Macro and microstructure of the weld at a rotation speed of 710 rpm and a travel speed of 1.5 rpm.

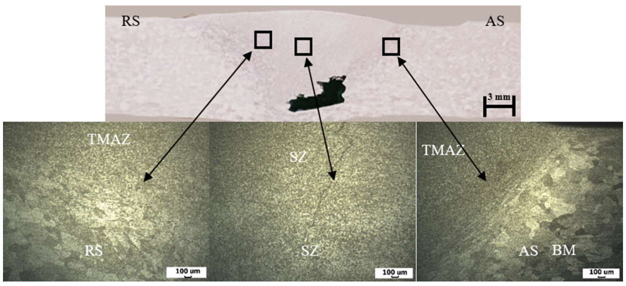

Fig. 8. Macro and microstructure of the weld at a rotation speed of 1000 rpm and a travel speed of 1.5 rpm.

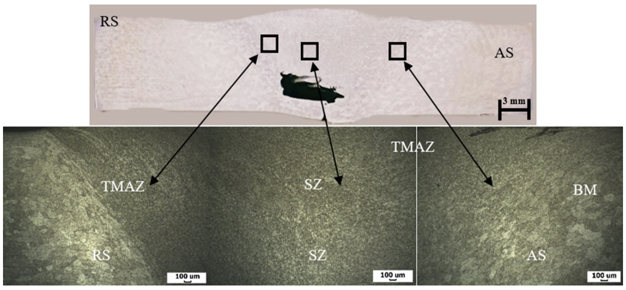

Fig. 9. Macro and microstructure of the weld at a rotation speed of 1400 rpm and a travel speed of 1.5 rpm.

Microstructural analysis of the welds at a rotation speed of 710 rpm revealed small cracks in the Stir Zone (SZ) region. This phenomenon was attributed to excessive frictional heat accumulation between the material and the welder, leading to stress that resulted in cracks and tunnels within the material [11]. Additionally, no cracks were observed in the Thermo-Mechanically Affected Zone (TMAZ) on either the Advancing Side (AS) or Retreating Side (RS). However, the grain shape in these regions was severely distorted and elongated, giving the appearance of being dragged. This distortion was caused by the rotation of the welder, which had an immediate impact on both the material and the overall structure.

Considering the microstructure of the welds at higher rotation speeds (between 1000 and 1400 rpm), it was observed that the grains in the Stir Zone (SZ) were finer and smaller compared to those at the lower rotation speed of 710 rpm. This refinement occurred due to the increased compression exerted by the rotating pin, which led to a higher accumulation of heat in the material within the SZ. This process resulted in dynamic recrystallization (DRX) during friction stir welding. Furthermore, a closer examination of the Thermo-Mechanically Affected Zone (TMAZ) on both the Advancing Side (AS) and Retreating Side (RS) revealed more elongated and distorted grains, with these characteristics becoming more pronounced at the maximum rotation speed of 1400 rpm. This effect can be attributed to the nature of the friction stir welding technique, where the welder directly contacts the material while being rotated by the vertical milling machine's rotational force. As the rotational force increases, the material in a plastic state moves in the direction of this force, resulting in a material structure that rotates in unison with the welder.

One intriguing aspect of the microstructure was the continuous connection between the macrostructure and the microstructure, which was influenced by defects such as voids or tunnels along the weld line. Conversely, these cracks were not visible at the macroscopic level. In this study, the lengths of the cracks in the Stir Zone (SZ) region increased significantly from low rotation speed (710 rpm) to high rotation speed (1400 rpm). Notably, the crack length was considerably greater at the 710 rpm rotation speed compared to the lengths observed at 1000 and 1400 rpm. This variation impacted the tensile strength, which will be discussed later. The phenomenon can be attributed to excessive dynamic recrystallization (DRX), which facilitated the crystallization of grains in the SZ region, coupled with the material's exposure to excessive stress that ultimately resulted in crack formation [8].

For the macro and microstructure of the weld cross-section, the macrostructure in the SZ region exhibited a distinct onion ring shape, which became more pronounced when a threaded welder was used [12]. This was because the threaded welder generated more heat, placing the material in a plastic state and forming smaller onion rings in the SZ region. Additionally, the threads enhanced material flow by efficiently directing it along the welder's threads and pins. With increased heat, the threaded welder effectively regulated material flow, improving thermal softening and enhancing material movement along the thread surface compared to a non-threaded welder.

Furthermore, the threaded welder produced a more stable material flow, likely due to the threads on its surface. Dynamic recrystallization during welding resulted in a consistent grain morphology and an increase in average grain diameter. The grains formed with the threaded welder were finer than those produced by the non-threaded welder due to improved plastic flow along the thread surface. The increased heat led to a larger heat input, resulting in higher peak temperatures and longer cooling times [13, 14], which extended the material's heat exposure. Under such conditions, aluminum alloys typically experience enhanced grain growth, leading to an increase in grain size.

These findings align with previous research indicating that welders with different pin geometries significantly influence microstructural characteristics, such as grain size, orientation in the SZ region, heat accumulation along the weld line, stress distribution, and material flow in various plastic states around the welder's pins [15]. Additionally, a study by Salih et al. [16] found that the threaded welder produced a more homogeneous microstructure, finer grain structure, and enhanced dynamic recrystallization. This was attributed to the greater friction and agitation generated by the threaded welder compared to the non-threaded version.

Fig. 10 displays the macrostructure of the welds at different rotation and travel speeds. Defects formed in the Stir Zone (SZ) region of the welds due to insufficient heat or friction during the welding process, which prevented the metals from fusing properly. As the rotation and travel speeds increased, the tunnels in the welds became wider. This phenomenon occurred because the weld was unable to generate and retain sufficient heat when the pin first started rotating. Excessive rotation speed and high travel speed of the welder resulted in abnormal material stirring and a high temperature gradient in the thickness direction. Such abnormal stirring led to flow separation, creating a gap on the Advancing Side (AS). At low rotation speeds combined with high travel speeds, tunnels primarily formed due to inadequate heat input. It has been noted that tunnels in welds are often caused by insufficient axial force and improper tool design [17, 18]. Interestingly, wider tunnels were observed on the retreating side in the SZ region of the welds at higher travel speeds. This was likely due to friction between the pin and the material, along with inadequate heat accumulation during welding. The material did not undergo plastic deformation when the welding commenced at the designated travel speed, which hindered the material from flowing to different locations at the specified rotation speed [19].

Tunnel formation can be mitigated by maintaining an appropriate heat generation rate, ensuring even heat distribution on both sides of the joint, and facilitating proper material accumulation at the back of the welder during movement. Additionally, sufficient rotation speed and a low travel speed of the friction stir welder promote high heat input and optimal material flow in the mixing zone [20].

Welder geometry also influences tensile strength. As reported by Goel et al. (2018) [21], cylindrical and tapered pins produced continuous material flow, resulting in fine grains, improved material mixing, and consistent heat accumulation in the welds. These factors contributed to enhanced tensile strength compared to triangular pins, which exhibited reduced tensile strength due to tunnel defects in the welds. This highlights the importance of selecting an appropriate welder to minimize weld defects.

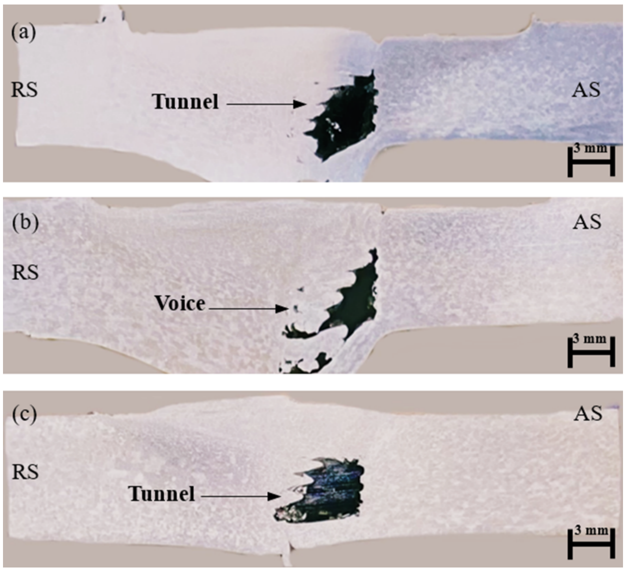

Fig. 10. Macrostructure of the welds.(a) Rotation speed of 700 rpm and travel speed of 3.5 rpm, (b) Rotation speed of 1000 rpm and travel speed of 3.5 rpm and (c) Rotation speed of 1400 rpm and travel speed of 3.5 rpm

Furthermore, Zhao et al. (2019) [22] developed a 3D thermofluid model to evaluate tunnel defects in the friction stir welding process. The model demonstrated that higher temperatures in the SZ region were associated with eddy currents generated during welder rotation, which helped reduce tunnel formation in the welds.

One notable defect in welds is cracking, which is influenced by thermal stress at the grain, grain boundaries, and interfaces between solid particles and the matrix. Large impurity particles often contribute to micro-crack formation [23]. To minimize crack formation, selecting optimal welding process conditions is essential [24].

Fig. 11(a) displays the microstructure of the weld as observed by scanning electron microscopy (SEM) at a rotation speed of 1000 rpm and a travel speed of 1.5 mm/min. The Stir Zone (SZ) region exhibited α-phase fracture throughout, as illustrated in the figure. The grains in this region were finer compared to those in the Thermo-Mechanical Affected Zone (TMAZ) because the weld was directly stirred by the pin. Furthermore, as shown in Fig. 11(b), the chemical composition analysis performed with an Energy Dispersive X-ray Analyzer (EDX) revealed that the predominant phase of the weld was aluminum (Al), with smaller amounts of silicon (Si) and magnesium (Mg) phases distributed along the weld's structure. The quantitative elemental analysis, depicted in Fig. 11(c), indicated that the weld contained 99.1% aluminum (Al), 0.5% magnesium (Mg), and 0.4% silicon (Si).

Fig. 12 illustrates the simulated temperature distribution in the specimens when the welder tool rotated clockwise while the specimens moved counterclockwise. Fig. 12(a) presents the full mesh modeling setup using the adaptive meshing method in SolidWorks 2020, which employed 16 Jacobian points for high-quality meshing with an element size of 6.32 mm and a tolerance of 0.31 mm. The meshing process resulted in a total of 96,331 nodes and 51,213 elements.

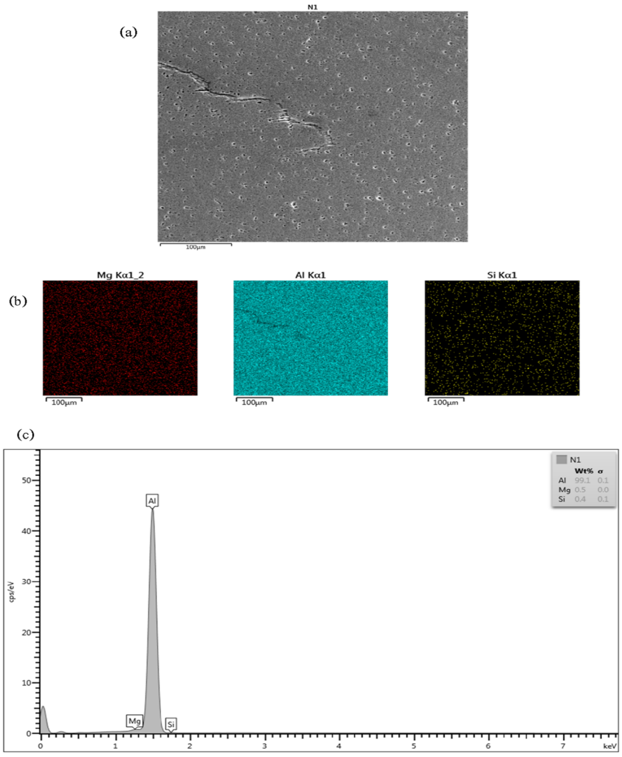

Fig. 11. SEM and EDX of the welds.(a) Scanning electron microscopy (b) Mapping analysis and (c) Qualitative element analysis

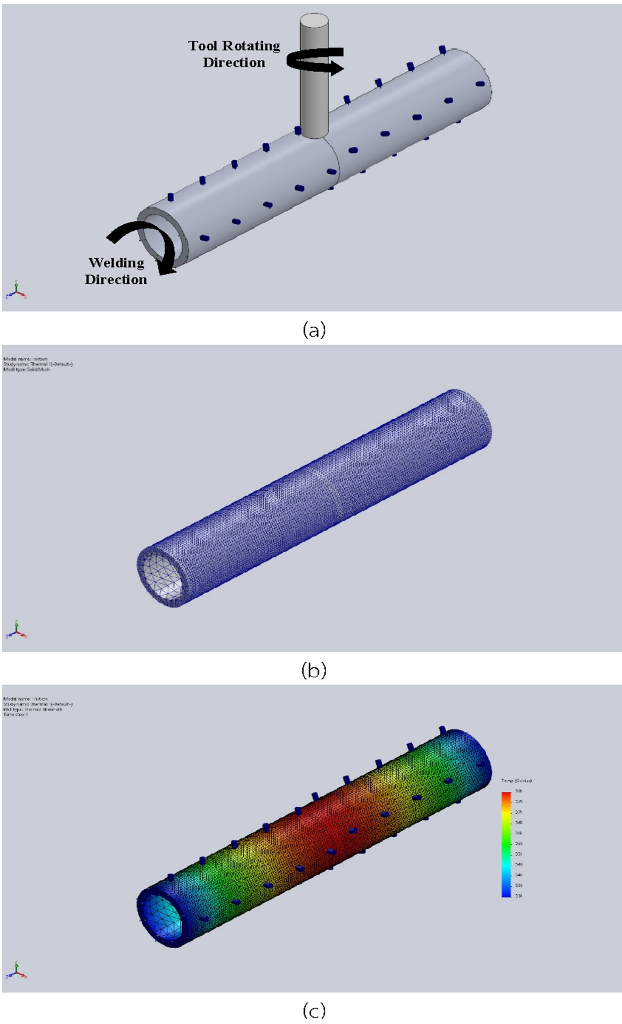

Fig. 12. Simulation of temperature distribution in specimen (a) 3D geometric model of welder and specimen used in simulation, (b) Geometric model of specimen used in simulation and (c) Temperature distribution model of specimen

Fig. 12(b) depicts the simulated temperature distribution during welding. Due to excessive frictional heat generation and permanent deformation near the welder, a heat-affected zone (HAZ) formed around the tool. The temperature at the center of the weld on the forward side reached 383 °C. Friction stir welding produced elevated temperatures around the welder, particularly on its forward and backward sides, which subsequently reduced material flow force [25]. This reduction in force enhanced material softening in both the forward and backward directions, thereby facilitating material flow, as shown in Fig. 12(c).

3.3 Tensile strength of the welds

The comparison of tensile strengths of the welds revealed that the highest tensile strength, measuring 152.17 MPa, was observed at a rotation speed of 1000 rpm and a travel speed of 1.5 mm/min. Conversely, the lowest tensile strength, at 141.65 MPa, occurred at a rotation speed of 1400 rpm and a travel speed of 3.5 mm/min. The results of the experiments conducted under various conditions are presented in Fig. 13.

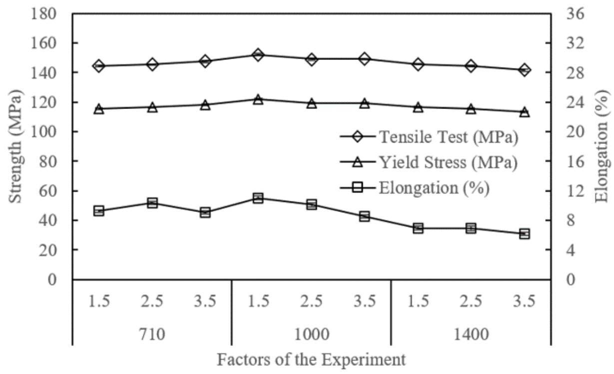

Fig. 13. Tensile strength of the welds under all conditions of friction stir welding.

Analyzing the tensile strength, it was found that tensile strength increased as the rotation speed rose from 710 rpm to 1000 rpm. However, a further increase in rotation speed to 1400 rpm resulted in a decrease in tensile strength. This reduction in tensile strength was influenced by the microstructure, as more tunnels formed in the welds at higher rotation speeds, aligning with findings reported in reference [26]. Additionally, the increase in rotation speed led to material softening in the Stir Zone (SZ), which directly impacted the weld strength.

Fig. 13 displays the tensile strength graph of the welds produced under all conditions of friction stir welding in this study. From this figure, it can be observed that the weld joint efficiency was 67.63% when compared to the highest tensile strength, but only 59.02% when compared to the lowest tensile strength, based on the original metal strength of 225 MPa. The comparatively low tensile strength can be attributed to weld defects, particularly tunnels, which are among the most common defects encountered during the friction stir welding (FSW) process. Tunnels formed due to inadequate material flow from the Retreating Side (RS) to the Advancing Side (AS) as a result of the welder's inappropriate size [17].

Achieving a flawless weld also necessitates intermittent material flow from a specified region around the pin and beneath the shoulder [27]. Additionally, optimal weld strength is achieved when the grains crystallize properly without the formation of cracks. Meanwhile, it was noted that under all experimental conditions, the elongation did not reach 12%. This limitation was due to the presence of numerous weld defects and inconsistent welding variables, which resulted in the previously described test outcomes.

3.4 Weld hardness

Fig. 14-16 illustrate the weld hardness at rotation speeds of 710, 1000, and 1400 rpm, along with travel speeds of 1.5, 2.5, and 3.5 mm/min, respectively.

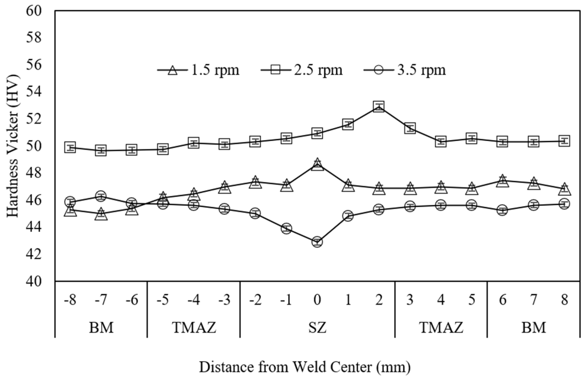

Fig. 14. Weld hardness at a rotation speed of 710 rpm.

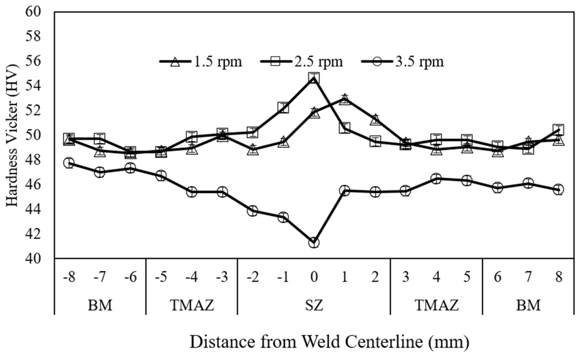

Fig. 15. Weld hardness at a rotation speed of 1000 rpm.

Fig. 14 presents the weld hardness at a rotation speed of 710 rpm. The highest hardness recorded in the Stir Zone (SZ) was 52.9 HV at a travel speed of 2.5 mm/min, while the lowest hardness of 42.9 HV was observed at a travel speed of 3.5 mm/min.

Fig. 15 displays the weld hardness at a rotation speed of 1000 rpm. The highest hardness in the Stir Zone (SZ) was measured at 54.6 HV at a travel speed of 2.5 mm/min, whereas the lowest hardness of 41.3 HV was noted at a travel speed of 3.5 mm/min.

Fig. 16 illustrates the weld hardness at a rotation speed of 1400 rpm. The highest hardness in the Stir Zone (SZ) was found to be 57.3 HV at a travel speed of 2.5 mm/min, while the lowest hardness of 46.1 HV was recorded at a travel speed of 3.5 mm/min.

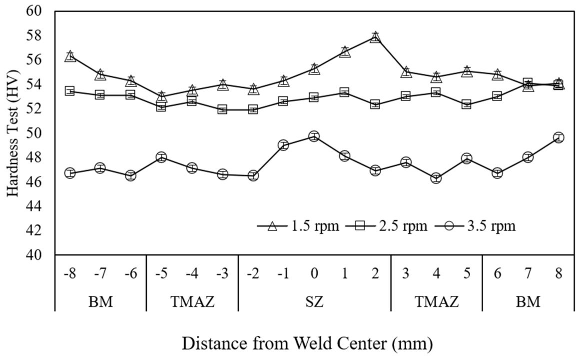

Fig. 16. Weld hardness at a rotation speed of 1400 rpm.

The rotation speed and travel speed exhibited different effects on weld hardness. Notably, most hardness values were close to that of the original metal, primarily due to the reduction in hardness within the Stir Zone (SZ), which was influenced by the accumulation of frictional heat between the specimen and the shoulder [28]. When the temperature in the SZ exceeded the eutectic temperature, the material softened, resulting in decreased hardness. Consequently, the highest hardness recorded in this experiment was 57.3 HV at a rotation speed of 1400 rpm and a travel speed of 2.5 mm/min, while the lowest hardness observed was 41.3 HV at a rotation speed of 1000 rpm and a travel speed of 3.5 mm/min.

3.5 General factorial statistical analysis

The statistical analysis of tensile testing was conducted using the General Factorial Regression method with two experimental factors: rotation speed (710, 1000, and 1400 rpm) and travel speed (1.5, 2.5, and 3.5 rpm). The objective was to evaluate the effects of these parameters on the tensile strength of the welds. The results are presented in Table 2.

Table 2. Statistical analysis of tensile strength of the welds.

Source	DF	Adj SS	Adj MS	F-Value	P-Value
Model	8	401.20	50.150	144.04	0.000
Linear	4	310.13	77.533	222.69	0.000
Rotation Speed (rpm)	2	296.05	148.023	425.16	0.000
Welding Speed (rpm)	2	14.09	7.043	20.23	0.000
2-Way Interactions	4	91.07	22.767	65.39	0.000
Rotation Speed*Welding Speed	4	91.07	22.767	65.39	0.000
Error	36	12.53	0.348		
Total	44	413.73			
S = 0.590051	R-Sq = 96.97%		R-Sq(adj) = 96.30%	R-sq(pred) = 95.27%	

The analysis of tensile strength for welds produced at various rotation and travel speeds (Tab. 2) showed a coefficient of determination (R^2) of 96.30%. This indicates that controllable factors, such as the welder, equipment, and constant parameters, accounted for 96.30% of the experimental variation, while uncontrollable factors contributed 3.70%. Since the R^2 value exceeded 70%, the experimental design was considered appropriate.

Since the p-value was less than 0.05, both rotation speed and travel speed had a significant effect on the tensile strength of the welds.

The analysis of the main effects of friction stir welding revealed that both rotation speed and travel speed influenced the tensile strength of the welds. As shown in Fig. 17, tensile strength increased with higher rotation speed. However, beyond a certain point, further increases in rotation speed led to a decrease in tensile strength. The experimental data confirmed the significant effect of rotation speed on tensile strength at a 95% confidence level.

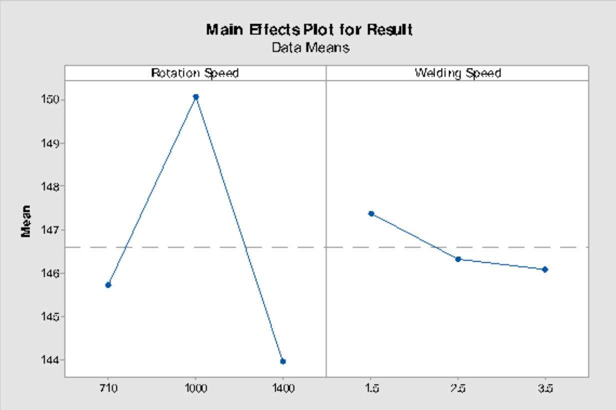

Fig. 17. Main effects of friction stir welding.

Regarding travel speed, tensile strength steadily declined as travel speed increased up to its maximum value. The experimental data also confirmed that travel speed significantly affected tensile strength at a 95% confidence level.

At a rotation speed of 710 rpm, the analysis of the interaction effects in friction stir welding of pipes showed that tensile strength increased with travel speed. However, at rotation speeds of 1000 and 1400 rpm, tensile strength decreased as travel speed increased. The experimental data confirmed a significant interaction effect between rotation speed and travel speed at a 95% confidence level. The results are shown in Fig. 18.

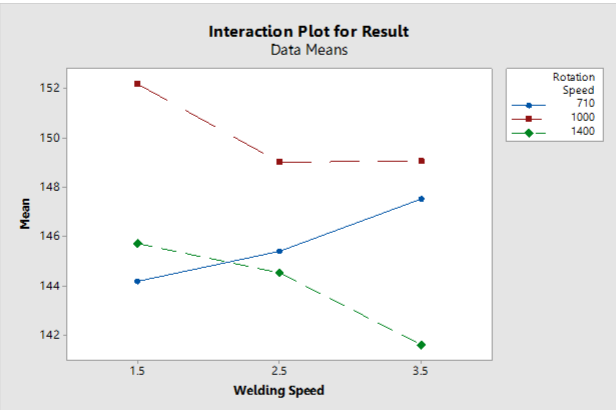

Fig. 18. Interaction effects of friction stir welding.

This study investigated the friction stir welding of 6063 aluminum pipes using a novel approach that employs a specialized welder mounted on a conventional milling machine. This method is practical and cost-effective, eliminating the need for large, expensive specialized machinery. Additionally, the friction stir welder can accommodate pipes of various diameters, making it a versatile solution. Furthermore, welding parameters can be optimized for different materials, allowing for broader applications in industrial settings.

4. Conclusion

The friction stir welder is equipped with an inverter and a motor that allows for automatic adjustment of the rotation speed of the dividing plate. This welder is capable of performing friction stir welding on pipes with diameters ranging from 25 to 100 mm.

The surface of the welds demonstrated good integration of the butt welds, with the bottom of the welds exhibiting effective penetration and no signs of non-integrated cracks. However, holes were observed at the ends of the welds, attributed to the tip of the pin.

Small cracks were identified in the Stir Zone (SZ) of the welds. This was caused by excessive accumulation of frictional heat between the material and the welder, leading to stress that resulted in tunnels within the material.

Excessive rotation speed and high travel speed of the welder resulted in abnormal material stirring and a steep temperature gradient in the thickness direction. This abnormal stirring led to flow separation, creating gaps on the advancing side (AS). Conversely, at low rotation speed combined with high travel speed, tunnels formed primarily due to insufficient heat input.

Friction stir welding conducted at a rotation speed of 1000 rpm and a travel speed of 1.5 mm/min achieved the highest tensile strength, measuring 152.17 MPa.

The experiment identified the highest hardness value of 57.3 HV at a rotation speed of 1400 rpm and a travel speed of 2.5 mm/min.

Acknowledgements
This research was financially supported by the Science, Research, and Innovation Promotion Fund (SRI) through the budget allocation for the year 2024, as part of the Strategic Plan for Research and Innovation Development at Rajamangala University of Technology Srivijaya.

References

[1] S. Gain, S. K. Das, S. K. Acharyya and D. Sanyal, “Friction stir welding of industrial grade AISI 316L and P91 steel pipes: A comparative investigation based on mechanical and metallurgical properties,” *Int. J. Press. Vessels. Pip.*, vol. 201, Feb. 2023, Art. No. 104865, doi: 10.1016/j.ijpvp.2022.104865.
[2] C. Gurel and S. Mistikoglu, “Recent Developments in Friction Stir Welding of Al-Alloys,” *J. Mater. Eng. Perform.*, vol. 23, pp. 1936–1953, Apr. 2014, doi: 10.1007/s11665-014-0968-x.
[3] R. Jain *et al.*, “Friction Stir Welding: Scope and Recent Development,” in *Modern Manufacturing Engineering*, J. P. Davim, Ed., in Materials Forming, Machining and Tribology., Cham: Springer International Publishing, 2015, pp. 179–229. doi: 10.1007/978-3-319-20152-8_6.
[4] D. H. Lammlein, B. T. Gibson, D. R. DeLapp, C. Cox, A. M. Strauss and G. E. Cook, “The friction stir welding of small-diameter pipe: an experimental and numerical proof of concept for automation and manufacturing,” *Proc. Inst. Mech. Eng. B: J. Eng. Manuf.*, vol. 226, no. 3, pp. 383–398, Feb. 2023, doi: 10.1177/0954405411402767.
[5] B. Chen, K. Chen, W. Hao, Z. Liang, J. Yao, L. Zhang, and A. Shan, “Friction stir welding of small-dimension Al3003 and pure Cu pipes,” *J. Mater. Process. Technol.*, vol. 223, pp. 48–57, Sep. 2015, doi: 10.1016/j.jmatprotec.2015.03.044.

[6] D. G. Hattingh, L. G. Von Welligh, D. Bernard, L. Susmel, R. Tovo and M. N. James, "Semiautomatic friction stir welding of 38 mm OD 6082-T6 aluminium tubes," *J. Mater. Process. Technol.*, vol. 238, pp. 255–266, Dec. 2016, doi: 10.1016/j.jmatprotec.2016.07.027.

[7] Y. Guo, X. He, C. Liu, C. Wei, R. Yang and X. Dong, "Study on the effects of ultrasonic assistance and external heat dissipation on friction stir welded 7075 aluminum alloy joints," *J. Manuf. Process.*, vol. 107, pp. 280–293, Dec. 2023, doi: 10.1016/j.jmapro.2023.10.046.

[8] S. Youbao, Y. Xinqi, C. Lei, H. Xiaopeng, S. Zhikang and X. Yan. "Defect features and mechanical properties of friction stir lap welded dissimilar AA2024-AA7075 aluminum alloy sheets," *Mater. Des.*, vol. 55, pp. 9–18, Mar. 2014, doi: 10.1016/j.matdes.2013.09.062.

[9] L. Luo, B. H. Yang, X. R. Yang, W. W. Yan, C. Gan, X. Y. Liu and J. Z. Wang. "Effects of different cooling conditions on microstructure and precipitation behavior of fine-grained Al-Zn-Mg-Cu alloy friction stir welding joint," *J. Mater. Res. Technol.*, vol. 24, pp. 4534–4550, May 2023, doi: 10.1016/j.jmrt.2023.04.052.

[10] B. Safarbali, M. Shamanian and A. Eslami, "Effect of post-weld heat treatment on joint properties of dissimilar friction stir welded 2024-T4 and 7075-T6 aluminum alloys," *Trans. Nonferrous. Met. Soc. China*, vol. 28, no. 7, pp. 1287–1297, Jul. 2018, doi: 10.1016/S1003-6326(18)64766-1.

[11] H. J. Aval and M. F. Naghibi, "Orbital friction stir lap welding in tubular parts of aluminium alloy AA5083," *Sci. Technol. Weld. Join.*, vol. 22, no. 7, pp. 562–572, Jan. 2017, doi: 10. 1080/13621718.2016.1275099.

[12] A. Banik, B. S. Roy, J. D. Barma and S. C. Saha, "An experimental investigation of torque and force generation for varying tool tilt angles and their effects on microstructure and mechanical properties: Friction stir welding of AA 6061-T6," *J. Manuf. Process.*, vol. 31, pp. 395–404, Jan. 2018, doi: 10.1016/j.jmapro.2017.11.030.

[13] R. S. Mishra and Z. Y. Ma, "Friction stir welding and processing," *Mater. Sci. Eng.: R. Rep.*, vol 50, no. (1–2), pp. 1–78, Aug. 2005, doi: 10.1016/j.mser.2005.07.001.

[14] M. M. Attallah and H. G. Salem, "Friction stir welding parameters: a tool for controlling abnormal grain growth during subsequent heat treatment," *Mater. Sci. Eng.*, vol. 391, no. 1–2, pp. 51–59, Jan. 2005, doi: 10.1016/j.msea.2004.08.059.

[15] A. Garg, M. Raturi and A. Bhattacharya, "Strength, failure and microstructure development for friction stir welded AA6061-T6 joints with different tool pin profiles," *CIRP J. Manuf. Sci. Technol.*, vol. 29, pp. 99–114, May. 2020, doi: 10.1016/j.cirpj.2020.03.001.

[16] O. S. Salih, H. Ou, X. Wei and W. Sun, "Microstructure and Mechanical Properties of Friction Stir Welded AA6092/SiC Metal Matrix Composite," *Mat. Sci. Eng. A.*, vol. 742, pp. 78–88, Jan. 2019, doi: 10.1016/j.msea.2018.10.116.

[17] X. C. Liu and C. S. Wu, "Elimination of tunnel defect in ultrasonic vibration enhanced friction stir welding," *Mater. Des.*, vol. 90, pp. 350–358, Jan. 2016, doi: 10.1016/j.matdes.2015.10.131.

[18] M. Dehghani, A. Amadeh and S. A. A. Akbari Mousavi, "Investigations on the effects of friction stir welding parameters on intermetallic and defect formation in joining aluminum alloy to mild steel," *Mater. Des.*, vol. 49, pp. 433–441, Aug. 2013, doi: 10.1016/j.matdes.2013.01.013.

[19] M. F. Naqibi, M. Elyasi, H. J. Aval and M. J. Mirnia, "Theoretical and experimental studies on fabrication of two-layer aluminum-copper pipe by friction stir additive manufacturing," *Trans. Nonferrous Met. Soc. China*, vol. 31, no. 12, pp. 3643–3658, Dec. 2021, doi: 10.1016/S1003-6326(21)65754-0.

[20] D. Das, S. Bag, S. Pal and A. De, "A review on phenomenological model subtleties for defect assessment in friction stir welding," *J. Manuf. Process.*, vol. 120, pp. 641–679, Jun. 2024, doi: 10.1016/j.jmapro.2024.04.063.

[21] P. Goel, A. N. Siddique, N. Z. Khan, M. A. Hussain, Z. A. Khan, M. H. Abidi, and A. Al-Ahmari, "Investigation on the Effect of Tool Pin Profiles on Mechanical and Microstructural Properties of Friction Stir Butt and Scarf Welded Aluminium Alloy 6063," Metals, vol. 8, no. 1, pp. 1–15, Jan. 2018, doi: 10.3390/met8010074.

[22] Y. Zhao, J. Han, J. P. Domblesky, Z. Yang, Z. Li and X. Liu, "Investigation of void formation in friction stir welding of 7N01 aluminum alloy," *J. Manuf. Process.*, vol. 315, pp. 139–149, Dec. 2019, doi: org/10.1016/j.jmapro.2018.11.019.

[23] H. Jian, Y. Wang, X. Yang and K. Xiao, "Microstructure and fatigue crack growth behavior in welding joint of Al-Mg alloy," *Eng. Fail. Anal.*, vol. 120, Feb. 2021, Art. No. 105034, doi: org/10.1016/j.engfailanal.2020.105034.

[24] V. P. Singh, S. K. Patel, N. Kumar and B. Kuriachen, "Parametric effect on dissimilar friction stir welded steel-magnesium alloys joints: a review," *Sci. Technol. Weld. Join.*, vol. 24, no. 8, pp. 653–684, Nov. 2019, doi: org/10.1080/13621718.2019.1567031.

[25] L. Long, G. Chen, S. Zhang, T. Liu and Q. Shi, "Finite-element analysis of the tool tilt angle effect on the formation of friction stir welds," *J. Manuf. Process.*, vol. 30, pp. 562–569, Dec. 2017, doi: org/10.1016/j.jmapro.2017.10.023.

[26] S. M. Senthil, and M. B. Kumar, "Effect of Tool Rotational Speed and Traverse Speed on Friction Stir Welding of 3D-Printed Polylactic Acid Material," *Appl. Sci. Eng. Prog.*, vol. 15, Jan.–Mar. 2022, Art. No. 5403, doi: 10.14416/j.asep.2021.09.002.

[27] W. J. Arbegast, "A flow-partitioned deformation zone model for defect formation during friction stir welding," *Scr. Mater.*, vol. 58, no. 5, pp. 372–376, Mar. 2008, doi: 10.1016/j.scriptamat.2007.10.031.

[28] D. G. Hattingh, L. G. Von Welligh, D. Bernard, L. Susmel, R. Tovo, and M. N. James, "Semiautomatic friction stir welding of 38 mm OD 6082-T6 aluminium tubes," *J. Mater. Process. Technol.*, vol. 238. pp. 255–266, May 2016, doi:10.1016/j.jmatprotec.2016.07.027.